CrystEngComm

Accepted Manuscript

ROYAL SOCIETY OF CHEMISTRY

www.rsc.org/crystengcomm

CrystEngComm

ARTICLE

Cocrystals of the Antiandrogenic Drug Bicalutamide: Screening, Crystal Structures, Formation Thermodynamics and Lattice Energies

Received 00th January 20xx,
Accepted 00th January 20xx

DOI: 10.1039/x0xx00000x

www.rsc.org/

Artem O. Surov,[a] Katarzyna A. Solanko,[b] Andrew D. Bond,[b§] Annette Bauer-Brandl,[b] German L. Perlovich[a]

Two new cocrystals of the non-steroidal anti-androgen drug bicalutamide (**Bic**) are reported with benzamide (**BZA**) and salicylamide (**2OHBZA**), both in a 1:1 molar ratio. X-ray crystal structure analysis shows that both cocrystals contain a folded molecular conformation of bicalutamide, similar to that seen in polymorph II of the pure drug. Calculations of intermolecular interaction energies using the PIXEL approach indicate closely comparable total lattice energies for [**Bic**+**BZA**] and [**Bic**+**2OHBZA**]. The structures are dominated by dispersion interactions, with a significant contribution also from the Coulombic, particularly in [**Bic**+**BZA**]. The main difference between the two cocrystals is seen for the bicalutamide–cocrystal former interaction energy, which is calculated to be slightly more stabilizing in [**Bic**+**BZA**]. The melting temperatures of the cocrystals (132 °C for [**Bic**+**BZA**] and 157 °C for [**Bic**+**2OHBZA**]) are significantly lower than that of the pure API (193 °C). In general, the melting temperatures of all known bicalutamide cocrystals are shown to increase with an increase of the total van der Waals volume (V_{vdw}) of the molecules in the asymmetric unit of the crystal. The thermodynamic functions of the cocrystal formation were estimated from the solubility of the cocrystals and the corresponding solubility of the pure compounds in chloroform at various temperatures. In both cases, the Gibbs energy of formation was found to be small: –3.4 kJ·mol–1 for [**Bic**+**BZA**] and –2.2 kJ·mol–1 for [**Bic**+**2OHBZA**]. The most significant contribution to the Gibbs energy is provided by the exothermic enthalpy of formation. However, the cocrystal formation is accompanied by a considerable decrease of the system entropy, which diminishes the overall driving force of the process. Both cocrystals demonstrated a classical "spring and parachute" behavior during aqueous dissolution, providing an increased concentration level of Bic compared to that of the parent drug for several hours.

1. Introduction

Bicalutamide (**Bic**) is a first-generation active non-steroidal antiandrogenic drug that is given by an oral route to treat prostate cancer.[1] (Figure 1). The drug competitively inhibits the action of androgens by binding to cytosol androgen receptors in the target tissue and blocks the growth stimulating effect of androgens on prostate cancer.[2] Therefore, it is widely used in the treatment of locally advanced and metastatic prostate cancer, either as a monotherapy or combined with other anticancer agents. According to the biopharmaceutical classification system (BCS), bicalutamide is classified as a class II drug having low water solubility and high permeability. Due to high lipophilicity and the poor aqueous solubility, the pharmacokinetics of the drug after oral administration are highly variable.[3,4] In addition, a high pKa value of 12 is responsible for the poor solubility of the drug in any physiological media, which is a main factor limiting the oral bioavailability.

Different strategies to improve the aqueous solubility and / or dissolution rate and thus absorption of the drug have been described in the literature, such as solid dispersions,[3, 5-9] particle size reduction,[10-12] development of various nanoparticulate delivery systems,[13-16] complexation with cyclodextrins.[17,18] An alternative approach to overcome the solubility challenge without modification of the pharmacophore structure of an active pharmaceutical ingredient (API) is to develop new crystalline forms such as polymorphs, solvates, salts or cocrystals. Two polymorphic forms of bicalutamide have been reported and their crystal structures, physico-chemical properties and thermodynamic stability have been investigated.[19,20] A solvate with dimethyl sulfoxide has been described by Perlovich et al.[21] It should be stressed that bicalutamide represents a good example of an API for which salt formation is limited due to lack of suitable ionizable groups. In this case,

[a,a] *Institution of Russian Academy of Sciences, G.A. Krestov Institute of Solution Chemistry RAS, 153045 Ivanovo, Russia. Fax: +7 4932 336237; Tel: +7 4932 533784; E-mail: glp@isc-ras.ru.*
[b,b] *Department of Physics, Chemistry and Pharmacy, University of Southern Denmark, Campusvej 55, 5230 Odense M, Denmark.*
[c, §] *Current address: University of Cambridge, Department of Chemistry, Lensfield Road, CB2 1EW, United Kingdom.*

Electronic Supplementary Information (ESI) available: list of cocrystal formers used for screening experiments, DSC results for the bicalutamide+cocrystal former physical mixtures, packing arrangements for the known bicalutamide cocrystals, solubility data for bicalutamide, benzamide, salicylamide and the corresponding cocrystals in organic solvents. See DOI: 10.1039/x0xx00000x

therefore, cocrystallization has great advantages since molecular cocrystals can be formed regardless of the API's ionisable status.[22,23] To date, however, cocrystal formation for bicalutamide does not seem to have been systematically explored, and only two cocrystals of **Bic** with 4,4′-bipyridine and trans-1,2- bis(4-pyridyl)ethene are known.[24] Unfortunately, these cocrystal formers may hardly be considered as a pharmaceutically relevant. Thus, development of novel crystalline forms of bicalutamide with potentially enhanced key physicochemical properties are still of considerable interest.

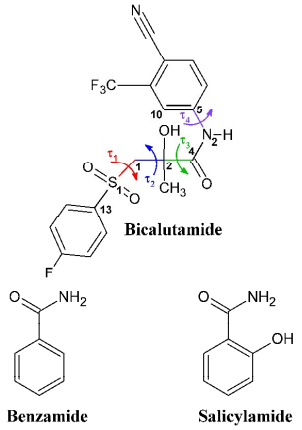

Figure 1 Molecular structures of bicalutamide, benzamide and salicylamide. The flexible torsion angles in the bicalutamide molecule are numbered and indicated by τ1, τ2, τ3 and τ4.

In this context, cocrystal screening of bicalutamide was conducted to extend the range of the API crystal forms. The cocrystals were characterized by single-crystal X-ray diffraction and differential scanning calorimetry. Aqueous dissolution, solution stability and formation thermodynamics of the cocrystals were also investigated. In addition, analysis of intermolecular interactions and crystal lattice energies of the cocrystals is made using the *PIXEL* approach.

2. Material and Methods

2.1. Compounds and solvents

Bicalutamide ($C_{18}H_{14}F_4N_2O_4S$, 99.8%) was produced by Xiamen Fine Chemical Import @ Export Co., Ltd. (Xiamen, China) and received as polymorphic form I, which is the most thermodynamically stable polymorph.[19] Solvents and cocrystal formers were purchased from various suppliers and used as received without further purification.

2.2 Screening procedures

2.2.1 Screening by Differential Scanning Calorimetry (DSC)

In the typical DSC screening experiment, a physical mixture of bicalutamide and a coformer were placed in a 2 mL test tube in 1:1 molar ratio and mixed with a vortex mixer for 1 min. The final mixture was immediately loaded to the aluminum pans and subjected to DSC analysis.

2.2.2 Liquid-Assisted Grinding

Liquid-assisted grinding experiments were performed using a Fritsch planetary micro mill, model Pulverisette 7, in 12 ml agate grinding jars with ten 5 mm agate balls at a rate of 600 rpm for 40 min. The experiments were carried out with 100 mg of bicalutamide and a cocrystal former in a 1:1 molar ratio and a few drops of solvent (acetone) added with a micropipette.

2.2.3 Slurry sonication

Approximately 80 mg amount of bicalutamide and the corresponding coformer in a 1:1 molar ratio was mixed in a 2 mL test tube with enough solvent (acetone) to give a wet paste. The mixture was sonicated at room temperature for 10 min at a maximum power[25-27]. The resulting solids were air-dried prior to analysis.

2.2.4 Solution crystallization

Bicalutamide (80 mg) was dissolved with the corresponding coformer in a 1:1 molar ratio in acetone, methanol or acetonitrile and stirred at room temperature until a clear solution was obtained. The resulting solution was filtered into a 2 ml test tube, covered by parafilm perforated with a few small holes, and allowed to evaporate slowly until a crystalline material was formed.

2.3. X-ray diffraction experiments

Single-crystal X-ray diffraction data were collected on a Bruker-Nonius X8-APEXII CCD diffractometer using MoKα radiation (λ = 0.7107 Å) at 150(1) K. The structures were solved by direct methods and refined by full matrix least-squares on F^2 with anisotropic displacement parameters for all non-hydrogen atoms.[28] The structure of [**Bic**+**BZA**] was refined as a 2-component twin. The twinning was identified using the *TWINROTMAT* module in *PLATON*,[29] and the final refinement was carried out against the generated HKLF-5 file. X-ray powder diffraction data (XRPD) were recorded under ambient conditions in Bragg-Brentano geometry with a Bruker D8 Advance diffractometer with CuKα_1 radiation (λ = 1.5406 Å).

2.4. DSC experiments

Thermal analysis was carried out using a *Perkin Elmer* DSC 4000 differential scanning calorimeter with a refrigerated cooling system. The sample was heated in sealed aluminum sample holders at the rate of 10 K·min^{-1} in a nitrogen atmosphere. The unit was calibrated with indium and zinc standards. The accuracy of the weighing procedure was ±0.01 mg.

2.5 Aqueous dissolution experiments

Dissolution measurements were carried out by the shake-flask method in a phosphate buffer with pH 7.4 at 25±0.1 °C. The excess amount of each sample was suspended in 10 ml of the buffer solution in Pyrex glass tubes. Aliquots of the suspension were withdrawn at predetermined intervals, filtered through a 0.22 μm PTFE syringe filter (Rotilabo®), and the content of the drug in the solution phase was determined by HPLC (see

section 2.7). The results are stated as the average of at least three replicated experiments.

2.6. Thermodynamics of the cocrystals formation

In the case of a (1:1) stoichiometry, the reaction of two-component compound formation from a pure API (A) and a pure coformer (B) may be described as

$$A_{solid} + B_{solid} \rightarrow AB_{solid} \quad (1)$$

It has been established in the literature that the standard free-energy change, ΔG_f^0, for the reaction given above may be expressed through the solubility data of each of the materials by the following equation:[30,31]

$$\Delta G_f^0 = -RT \cdot \ln\left(\frac{S_A^p \cdot S_B^p}{S_A^{cc} \cdot S_B^{cc}}\right) = -RT \cdot \ln\left(\frac{S_A^p \cdot S_B^p}{K_{sp}}\right) \quad (2)$$

where S_A^p and S_B^p are the solubility values of pure A and B in a solvent, and S_A^{cc} and S_B^{cc} are the solubility of the cocrystal components in a solution, when in equilibrium with the pure cocrystal. For the sake of simplicity, the activities of the components were approximated by molar concentrations. Solution complexation between the cocrystal components was neglected due to their low concentration. The product of S_A^{cc} and S_B^{cc} is generally known as K_{sp} of the cocrystal.

Comparison of equation (2) with the expression for the standard free-energy change for the isothermal reaction

$$\Delta G_f^0 = -RT \cdot \ln K_f \quad (3)$$

shows that the ratio appearing in the logarithmic term of equations (2) has the character of an equilibrium constant at the given temperature (and pressure). Therefore, this quantity can be defined as K_f. If the K_f values are known at different temperatures, the van't Hoff relation may be used to derive the formation enthalpy, ΔH_f^0, of a multi-component compound:

$$\frac{d \ln K_f}{d(1/T)} = -\frac{\Delta H_f^0}{R} \quad (4)$$

Finally, the entropy change of the formation process can be estimated from the general relationship relating different thermodynamic functions:

$$\Delta G_f^0 = \Delta H_f^0 - T \cdot \Delta S_f^0 \quad (5)$$

The bicalutamide cocrystals were found to be congruently soluble in chloroform. The solubility of the [**Bic**+**BZA**] (1:1) and [**Bic**+**2OHBZA**] (1:1) cocrystals and their constituents in this solvent was measured at 18.0, 22.0, 25.0 and 30.0 ± 0.1 °C. An excess of the solid was placed in a glass test tube and 2 ml of solvent was added. After 24 h of shaking, the suspension was filtered through a Rotilabo® syringe filter (PTFE, 0.2 μm), diluted by acetonitrile and the concentration of each compound in the saturated solutions at each temperature was analyzed by HPLC, as described in section 2.7. The results are stated as the average of at least three replicated experiments.

In order to estimate the solubility ratio between pure bicalutamide and pure coformers in common organic solvents (acetone, acetonitrile, methanol and ethyl acetate), solubility of the compounds was measured by a gravimetric method. In brief, the excess amount of the compound was suspended in 2 ml of the particular solvent and allowed to equilibrate under shaking at the 25°C during 24 hours. Then, 150 μl of the clear solution was transferred into a pre-weighed vial by micropipette. The vial was placed in a fume hood and the solvent was allowed to evaporate. The solid phases recovered after the solubility and remaining after evaporation was analyzed by DSC and XRPD to assure that no solid phase transformation occurs during the experiments.

2.7 High-Performance Liquid Chromatography (HPLC)

HPLC was performed on Shimadzu Prominence model LC-20AD equipped with a PDA detector and a C-18 column (150 mm × 4.6 mm i.d., 5μm particle size and 100 Å pore size). The flow rates of the mobile phases was 1 mL·min^{-1}. Elution of the samples from the phosphate buffer was achieved by a mobile phase consisting of methanol and water- 0.1% trifluoroacetic acid mixed in the 60:40 ratio (v/v) in an isocratic regime with UV detection at 271 nm. To analyze the samples from the chloroform solutions, a gradient method was used. The mobile phase consisted of (A) water- 0.1% trifluoroacetic acid and (B) acetonitrile. The following gradient was used for bicalutamide, salicylamide and the [**Bic**+**2OHBZA**] (1:1) cocrystal: a linear gradient from 30% to 80% B over 10 min, this composition was maintained for the next 5 min and then the percentage of the mobile phase component B was decreased from 80% to 30% for the next 10 minutes. For benzamide and the [**Bic**+**BZA**] (1:1) cocrystal, gradient elution was performed by changing the mobile phase from 15% to 80% B over 12 min, this composition was maintained for the next 3 min and then the percentage of the mobile phase component B was decreased from 80% to 15% for the next 12 minutes. The UV detection of bicalutamide, salicylamide and benzamide was carried out at wavelengths 271 nm, 301 nm and 224 nm, respectively. The concentrations were calculated according to an established calibration curve.

2.8 Crystal lattice energy calculations

Intermolecular interaction energies were calculated using the *PIXEL* approach developed by Gavezzotti.[32,33] This method provides quantitative determination of crystal lattice energies and pairwise intermolecular interactions, with a breakdown of these energies into coulombic, polarization, dispersion and repulsion terms. The molecular electron densities for the cocrystals were calculated at the MP2/6-31G** level of theory in the *GAUSSIAN09* program. All hydrogen atoms in the structures were set to the standard neutron values according to the default procedure in the *PIXEL* program.

3. Results and Discussion

3.1 Cocrystal screening of bicalutamide

There are several sites of hydrogen bonding in the bicalutamide molecule. The main proton donors are the hydroxyl (O–H) and amide (N–H) groups, while the carbonyl (C=O), sulfonyl (O=S=O) and cyan (C–N) groups act as proton acceptors. All of

the listed functional groups are seen to become involved in hydrogen bonding in polymorphic forms of the drug. Unfortunately, there are too few cocrystal structures of bicalutamide known to make any confident prediction concerning suitable cocrystal formers for the drug. Therefore, the cocrystal screening of bicalutamide was performed using a relatively broad set of compounds. The library was comprised of the aromatic carboxylic acids (benzoic and salicylic acids), their amides (benzamide, salicylamide and 4-hydroxybenzamide) and structurally related heterocyclic amides (nicotinamide, isonicotinamide and pyrazinamide) (Figure S1). These compounds offer different combinations of H-bond donor and H-bond acceptor groups capable of forming hydrogen-bonding interactions with the complementary sites in the bicalutamide molecule. In addition, most of the choosen coformers (**CF**s) are members of the GRAS list and have been employed previously for cocrystallization experiments with various APIs.

All the compounds under study (API and coformers) melt without decomposing. Therefore, for the preliminary screening, a DSC method was used as the most simple and rapid approach to select the systems which produce cocrystals. In this method, two individual components are mixed in stoichiometric proportions (1:1 molar ratio) and put in DSC crucibles. There are distinctive thermal events on the DSC curve, which are later analyzed to identify the cocrystal formation using the rules suggested by Lu et al.[34] and Yamashita et al.[35] According to these rules, components are capable of forming cocrystals if the following conditions are fulfilled: (a) the physical mixture melting produces at least two endothermic events corresponding to eutectic mixture and cocrystal melting (with their temperatures being different from the melting temperatures of individual components); (b) the eutectic melting (the first peak) is followed by a small exothermic effect.[36]

The DSC results for the Bic + CF physical mixtures showed that only the (bicalutamide + salicylamide) (1:1) system complied with the proposed rules for cocrystal formation (Figure S2a). The DSC curve of the mixture contains two distinct endo-peaks corresponding to the eutectic melting and the cocrystal melting, respectively. A small exo-event located between the endo-peaks is apparently responsible for cocrystal formation. For the rest of the physical mixtures, thermograms are found to be similar and generally contained one sharp endo-peak of the eutectic melting. For these systems, it was impossible to identify the presence or absence of a cocrystal based on DSC experiment solely, because the presence of only one peak on the melting curve does not imply that no cocrystal is formed (Figure S3a). Thus, alternative screening techniques need to be applied to support and verify the DSC results.

As a next step, liquid-assisted grinding experiments were carried out for all systems using acetone as a solvent. X-ray powder diffraction analysis of the ground materials confirmed the cocrystal formation between bicalutamide and salicylamide ([**Bic**+**2OHBZA**] (1:1)) (Figure S2b). In addition, a novel solid phase was identified in the mixture of bicalutamide with benzamide ([**Bic**+**BZA**] (1:1)) (Figure S3b). Any other cocrystal formers, however, were not seen to react with bicalutamide. Similar outcomes were observed after the slurry sonication and solution crystallization experiments (Table 1).

Table 1. Results of cocrystal screening of bicalutamide with 1:1 molar ratio[a]

Cocrystal former	DSC screening	Liquid-assisted grinding	Slurry sonication	Solution crystallization[b]	
Benzoic acid	–	–	–	–	ATN, MeOH, ACN
Salicylic acid	–	–	–	–	ATN, MeOH, ACN
Benzamide (BZA)	–	✔	✔	✔	ATN
				–	MeOH, ACN
Salicylamide (2OHBZA)	✔	✔	✔	✔	ATN
				–	MeOH, ACN
4-Hydroxybenzamide	–	–	–	–	ATN, MeOH, ACN
Nicotinamide	–	–	–	–	ATN, MeOH, ACN
Isonicotinamide	–	–	–	–	ATN, MeOH, ACN
Pyrazinamide	–	–	–	–	ATN, MeOH, ACN

[a]Symbol (–) stands for no cocrystal formation, (✔) for cocrystal.
[b]ATN – acetone, MeOH – methanol, ACN – acetonitrile.

The screening results suggest that the amide group of coformer is complementary to the H-bonding sites in the bicalutamide molecule. Moreover, formation of the cocrystal seems to depend on the number and spatial distribution of hydrogen-bond donor and acceptor functional groups in the coformer molecule. Inserting the hydroxy-fragment in the para-position of the benzamide molecule (4-hydroxybenzamide) or the substitution of the CH-group in the aromatic ring by the nitrogen heteroatom (nicotinamide, isonicotinamide, pyrazinamide) considerably alters the donor-acceptor properties of the molecule. It seems that the "excess" of the strong H-bond donors/acceptor in the cocrystal former and competition effects between them hinder cocrystal formation with bicalutamide.

3.2 Crystal structures and conformational analysis

Relevant crystallographic data for bicalutamide cocrystals are given in Table 2. In both structures, the asymmetric unit contains **Bic** and coformer molecules connected by two different hydrogen bonds (O1–H1···O5 and N3–H11···O3) to form a dimer with $R_2^2(10)$ graph set notation (Figure 2).[37,38] The second N3–H12···O3(O4) hydrogen bond between amide and sulfonyl groups of the molecules connects neighboring dimers into a closed-ring supramolecular tetrameric unit across a crystallographic inversion center that may be described in graph set notation as $R_4^2(8)$ for [**Bic**+**BZA**] and $R_4^4(12)$ for [**Bic**+**2OHBZA**] (Figure 2). The API and coformer molecules are additionally stabilized by the weak C20–H20···O4 interaction (Figure 2).

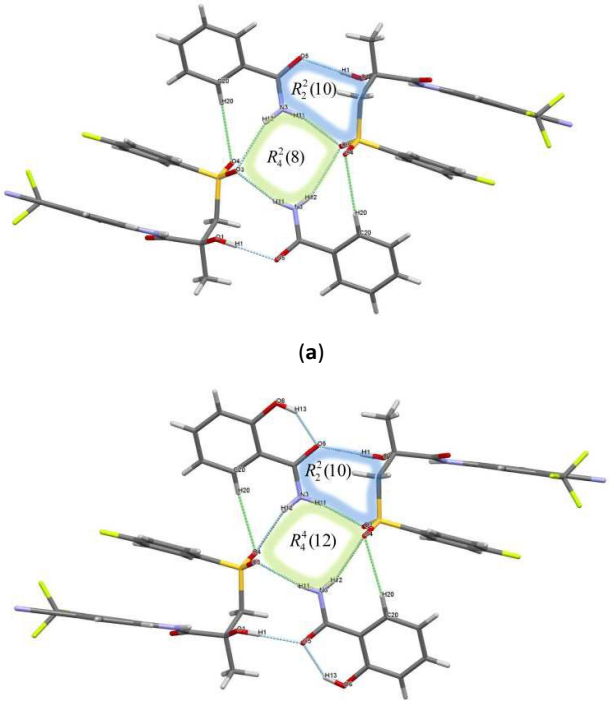

Figure 2 Hydrogen bonded molecular units in (**a**) [**Bic**+**BZA**] and (**b**) [**Bic**+**2OHBZA**] cocrystals.

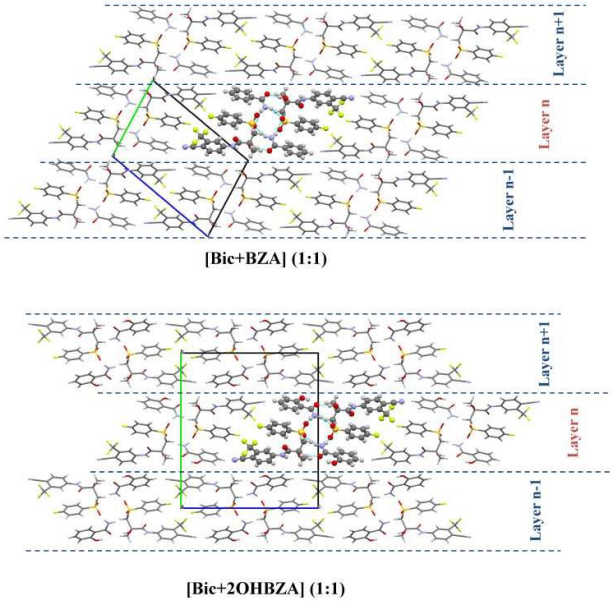

Figure 3 Molecular packing projections for [**Bic**+**BZA**] and [**Bic**+**2OHBZA**] cocrystals. The supramolecular tetrameric unit in the structures is shown in ball and stick style. The layers discussed in the text are separated by blue dashed lines.

In the crystals, the four-component units are packed in distinct parallel layers which can be seen in the (01-1) planes for [**Bic**+**BZA**] and the (020) planes for [**Bic**+**2OHBZA**] (Figure 3). In both structures, the bicalutamide molecule has a "folded" conformation, so that all the peripheral fluorine atoms are pointed to one side. This promotes a number of F···F and C–H···F contacts between the neighboring molecules located within the layer. Despite the similarity in packing arrangements, the cocrystals are not isostructural. Figure 3 shows that in [**Bic**+**BZA**], the adjacent layers are related by simple translation along the *b*-axis. In [**Bic**+**2OHBZA**], however, the units in the neighboring layers are related by 2-fold screw axis symmetry. The X-ray analysis indicates that conventional hydrogen bonding in the structures is limited to the tetrameric unit, while the rest of the crystal is mainly stabilized via weak non-directional intermolecular interactions. The description and energies of these interactions will be discussed subsequently.

Bicalutamide is known to be a flexible molecule, which displays a so-called conformational polymorphism in the solid state.[19] Comprehensive conformational analysis performed by Dhaked *et al.*[39] and Le *et al.*[10] using quantum chemical calculations has indicated that molecular conformations of **Bic** in polymorphs I and II belong to different energy minima separated by a relatively low energy barrier. The form II conformation, however, was found to be a relatively higher-energy state, at least in the gas phase.

Table 2. Crystallographic data for bicalutamide (**Bic**) cocrystals with benzamide (**BZA**) and salicylamide (**2OHBZA**)

Compound reference	[**Bic**+**BZA**] (1:1)	[**Bic**+**2OHBZA**] (1:1)
Chemical formula	$C_{18}H_{14}F_4N_2O_4S$•C_7H_7NO	$C_{18}H_{14}F_4N_2O_4S$•$C_7H_7NO_2$
Crystal system	Triclinic	Monoclinic
a/ Å	5.7985(11)	5.8888(3)
b/ Å	11.964(3)	21.5969(11)
c/ Å	17.496(3)	19.2814(10)
α/°	101.978(7)	90.00
β/°	97.828(7)	97.821(2)
γ/°	90.114(8)	90.00
Unit cell volume/ Å^3	1175.7(4)	2429.4(2)
Temperature/K	150(2)	150(2)
Space group	*P*–1	$P2_1/n$
No. of formula units per unit cell, *Z*	2	4
No. of reflections measured	9957	9776
No. of independent reflections	4022	3786
R_{int}	0.0417	0.0168
*R*1 ($I > 2\sigma(I)$)	0.0536	0.0300
*wR*2 (all data)	0.1308	0.0741
Goodness of fit on F^2	1.13	1.03
CCDC number	1474280	1474281

The molecule conformation of bicalutamide can be defined in terms of four torsion angles, three defining the conformation of the central spacer unit between the two rings (τ_1, τ_2 and τ_3) and one defining the orientation of the 4-cyano-3-(trifluoromethyl)phenyl ring (τ_4) (see Figure 1). The main conformational variations in the molecule are described by the torsion angle τ_1 (∠C2-C1-S1-C13), which is responsible for the mutual orientation of the different phenyl rings. The values of the selected torsion angles for the **Bic** molecule in all known

crystalline forms are collected in Table 3. The overlay of the molecular conformations is shown in Figure 4.

Table 3. Selected torsion angles τ1, τ2, τ3 and τ4 for bicalutamide in the known crystal forms

	τ_1,° (∠C13-S1-C1-C2)	τ_2,° (∠S1-C1-C2-C4)	τ_3,° (∠C1-C2-C4-N2)	τ_4,° (∠C4-N2-C5-C10)
Bic form I	-87.4	-64.9	131.6	153.5
Bic form II	72.5	-65.6	128.8	15.9
[**Bic+trans-1,2-bis(4-pyridyl)ethene**] (1:1)	141.5	-70.8	153.3	12.9
[**Bic+4,4'-bipyridine**] (1:1)	44.7	-83.2	131.9	10.9
[**Bic+DMSO**] (1:1)	-80.4	-67.2	133.8	1.9
[**Bic+BZA**] (1:1)	61.0	-68.5	128.0	7.1
[**Bic+2OHBZA**] (1:1)	60.5	-69.0	128.3	7.7

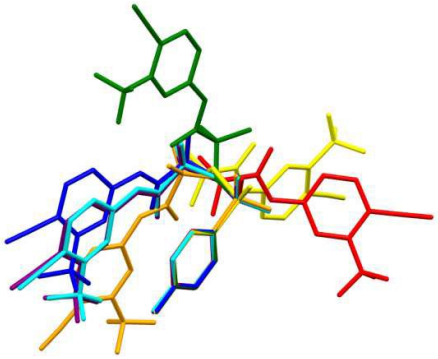

Figure 4 Overlay of bicalutamide conformations in the known crystal forms of the compound: **Bic** form I – red, **Bic** form II – blue, [**Bic+trans-1,2-bis(4-pyridyl)ethene**] (1:1) – green, [**Bic+4,4'-bipyridine**] (1:1) – orange, [**Bic+DMSO**] (1:1) – yellow, [**Bic+BZA**] (1:1) – cyan, [**Bic+2OHBZA**] (1:1) – purple. H atoms are omitted

Table 2 and Figure 4 shows that the molecular conformations of **Bic** in the [**Bic+BZA**] and [**Bic+2OHBZA**] cocrystals are virtually identical and found to be comparable to that in form II of pure bicalutamide and in the cocrystal with 4,4′-bipyridine (CSD: KIHZOR). It should be noted that the "folded" conformation of Bic seems to be more conformationally rigid compared to the "open" one which is observed in form I, the [**Bic+trans-1,2-bis(4-pyridyl)ethene**] cocrystal and the [**Bic+DMSO**] solvate. Table 2 shows clearly that each "open" molecular conformation has a unique set of the torsion angles τ1, τ2, τ3 and τ4. In the case of the "folded" conformation, all of the τ values in the different structures are generally comparable. This fact is seen to be a consequence of intramolecular π-π interactions between the phenyl rings of the molecule.

3.3 Crystal lattice energy calculations in the cocrystals

The intermolecular interaction energies in the cocrystals were analyzed according to the PIXEL approach developed by Gavezzotti.[32] The calculation results are summarized in Table 4. The calculations show that the total lattice energy for [**Bic+BZA**] is ca 4 kJ·mol-1 more stabilizing than that for the [**Bic+2OHBZA**] cocrystal. Such a small difference in the energy values is expected for the structurally similar cocrystals and found to be at the level of errors of the method (approximately 10%). However, PIXEL gives an opportunity not only to estimate the total lattice energy of the studied systems, but also to partition the total energy into electrostatic, polarization, dispersion and repulsion terms. Table 4 shows that the dispersion interactions dominate the structures of the cocrystals, while the Coulombic term also contributes significantly to the lattice energies, particularly in [**Bic+BZA**]. It should be noted that the main difference is observed for the Coulombic term (ca 20%), while the dispersion energy change does not exceed 6%. For the bicalutamide cocrystals with 4,4'-bipyridine, trans-1,2-bis(4-pyridyl)ethene and solvate with DMSO, the distribution of the energy terms is calculated to be similar to that in [**Bic+BZA**] and [**Bic+2OHBZA**], indicating that all of the crystals are mainly stabilized by van der Waals interactions.

Table 4. Results of PIXEL calculations (kJ·mol^{-1}): lattice energies (E_{latt}), coulombic (E_{coul}), polarization (E_{pol}), dispersion (E_{disp}) and repulsion (E_{rep}) terms

	E_{coul}	E_{pol}	E_{disp}	E_{rep}	E_{latt}
[**Bic+BZA**]	–234.7	–99.6	–278.7	310	–303.0
[**Bic+2OHBZA**]	–188.5	–76.0	–262.6	227.9	–299.2
[**Bic+4,4'-bipyridine**]	–172.4	–82.2	–253.0	216.3	–291.3
[**Bic+trans-1,2-bis(4-pyridyl)ethene**]	–185.3	–83.6	–289.7	239.8	–318.8
[**Bic+DMSO**]	–150.6	–71.2	–207.0	156.5	–272.3

Table 5 shows sums of the intermolecular interaction energies between the different types of molecules. In [**Bic+BZA**] and [**Bic+2OHBZA**], the **Bic-CF** interactions provide the largest contribution to the lattice energy (more than 60%). The **Bic-Bic** interactions comprise approximately a third of the total energy, while there is almost no interaction between the **CF** molecules. A similar relation between the **Bic-Bic** and **Bic-CF** relative contributions to the total energy (*ca* 30/60%) is also observed in the bicalutamide cocrystals with 4,4'-bipyridine and trans-1,2-bis(4-pyridyl)ethane. It seems that this fact can be attributed to similarity in the packing arrangements of the considered cocrystals. Indeed, in the [**Bic+4,4'-bipyridine**] and [**Bic+trans-1,2-bis(4-pyridyl)ethene**] cocrystals, the components generate supramolecular units consisting of two bicalutamide molecules and two coformer molecules linked by hydrogen bonds. Like in [**Bic+BZA**] and [**Bic+2OHBZA**], these units are found to be packed in distinct parallel layers (Figure S4a, S4b). The [**Bic+DMSO**] solvate also has a layer-like structure. In this case, however, the layers consist of **Bic** molecules only, and the solvent occupies the interlayer space (Figure S4c). As a result, the most significant contribution to the lattice energy of the solvate is made by the **Bic-Bic** interactions, while the **Bic-CF** interactions comprise approximately *ca* 40%.

As follows from Table 5, the main energy difference between the [**Bic+BZA**] and [**Bic+2OHBZA**] cocrystals is observed in the **Bic-CF** interactions (*ca* 3%), but the **Bic-Bic** and **CF-CF** interactions have closely comparable contributions to the total energy. In order to clarify the energy difference in the **Bic-CF** term, the strongest interactions of the central bicalutamide

molecule with the neighboring coformers in the crystal environment are shown in Figure 5a,b.

Table 5. Sums of the intermolecular interaction energies (kJ·mol^{-1}) between the different types of molecules calculated using the PIXEL method.

	Bic-Bic	Bic-CF	CF-CF	Total
[**Bic+BZA**]	–102.7 (33.9%)	–193.2 (63.8%)	–7.1 (2.4%)	–303.0
[**Bic+2OHBZA**]	–105.6 (35.3%)	–182.1 (60.9%)	–11.5 (3.8%)	–299.2
[**Bic+4,4'-bipyridine**]	–94.7 (32.5%)	–179.8 (61.7%)	–17.0 (5.8%)	–291.3
[**Bic+trans-1,2-bis(4-pyridyl)ethene**]	–101.8 (31.9%)	–183.6 (57.6%)	–33.6 (10.5%)	–318.8
[**Bic+DMSO**]	–142.1 (52.2%)	–117.4 (43.1%)	–12.9 (4.7%)	–272.3

In both structures, the interaction energies of **Bic** with the hydrogen-bonded coformer molecules (molecules **I** and **II**) are similar. The noticeable energy difference appears in the interactions of the central molecule with molecules **III** and **IV**. In [**Bic**+**BZA**], these **BZA** molecules are arranged almost perpendicularly to the plane of the 4-cyano-3-(trifluoromethyl)phenyl ring of **Bic** which promotes relatively strong C-H···π contacts. In [**Bic**+**2OHBZA**], the mentioned interactions are related to C–H···O and π···π contacts between the **2OHBZA** molecules and the 4-cyano-3-(trifluoromethyl)phenyl fragment of **Bic** with the energy values being smaller than in [**Bic**+**BZA**]. A significant difference is also observed for the interaction energies of the central molecule with molecule **VI**. Therefore, the *PIXEL* calculations suggest that the packing arrangement of [**Bic**+**BZA**] is slightly more favorable compared to that of [**Bic**+**2OHBZA**] in terms of the intermolecular interaction energies. In addition, comparison of the calculated densities and packing coefficients of the crystals indicates more efficient packing for the [**Bic**+**BZA**] structure than for [**Bic**+**2OHBZA**]: 1.603 g·cm^{-3}, 0.766 for [**Bic**+**BZA**] *cf* 1.552 g·cm^{-3}, 0.757 for [**Bic**+**2OHBZA**].

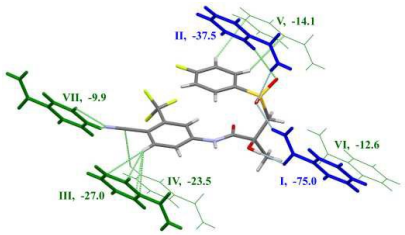

(**a**)

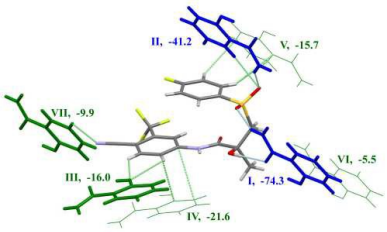

(**b**)

Figure 5. Strongest interactions between **Bic** and the neighbouring coformer molecules in (**a**) [**Bic**+**BZA**] and (**b**) [**Bic**+**2OHBZA**]. The hydrogen-bonded molecules are colored blue. The interaction energies are given in kJ·mol^{-1}.

3.4 Thermal analysis

DSC traces for the cocrystals and pure constituents are shown in Figure 6, and the thermal data are tabulated in Table 6. Our results for pure bicalutamide were in good agreement with the thermal analyses of the API reported previously.[20] DSC thermograms show only one major endotherm for the cocrystals which corresponds to the melting process, whereas other phase transitions are not observed. According to the DSC experiments, cocrystal formation leads to dramatic decreases of the melting point compared to the pure API. The melting temperature (T_{fus}) of [**Bic**+**BZA**] is *ca* 60°C lower than that of **Bic**, while for [**Bic**+**2OHBZA**], T_{fus} decreases by *ca* 36°C. However, the difference in melting points of the cocrystals themselves is less than 25°C. Similar thermal behavior is also observed for the bicalutamide cocrystals with 4,4'-bipyridine, trans-1,2-bis(4-pyridyl)ethene and solvate with DMSO.

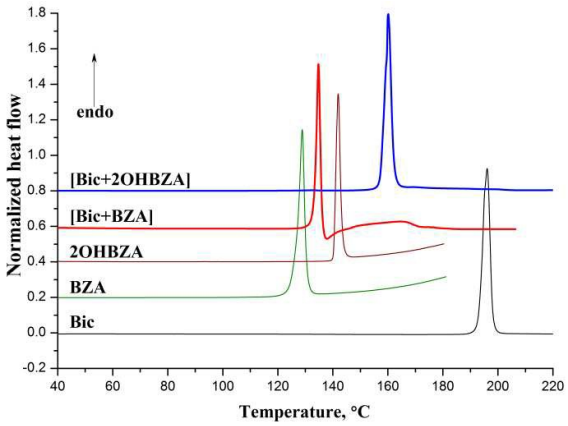

Figure 6 DSC curves for pure bicalutamide, benzamide, salicylamide and the cocrystals recorded at 10°C·min^{-1} heating rate.

Table 6. Thermophysical data for the bicalutamide cocrystals, coformers and total van der Waals volume of the molecules in the asymmetric unit

	T_{fus} (cocrystal)	ΔH_{fus} (cocrystal)	T_{fus} (coformer)	V_{vdw},
	°C	kJ mol^{-1}	°C	Å^3
[**Bic+BZA**]	132.4 ± 0.8	73.1 ± 1.8	127.7 ± 0.5	428.1
[**Bic+2OHBZA**]	157.2 ± 0.6	72.8 ± 1.6	140.6 ± 0.3	435.0
[**Bic+4,4'-bipyridine**][a]	163.0	-	151.0	482.8
[**Bic+trans-1,2-bis(4-pyridyl)ethene**][a]	159.0	-	112.0	459.6
[**Bic+DMSO**][b]	115.3	-	19.0	385.9
Bic	193.0 ± 0.4	51.0 ± 0.6	-	-

[a] Data taken from ref. 24;

[b] Data taken from ref. 21.

There are few examples of cocrystals in the literature, for which the melting temperatures change in any systematic way.[40-44] In

the recent work of Perlovich,[45] a set of correlation equations connecting the melting points of cocrystals and individual components has been derived based on statistical analysis of an extensive database. However, in most cases, prediction and interpretation of cocrystal thermal behavior remains a nontrivial task. For the bicalutamide cocrystals, we did not find clear relationship between melting points of the cocrystals and the respective coformers.

Since all of the bicalutamide cocrystals are mainly stabilized by van der Waals interactions, we have analyzed the influence of the total van der Waals volume (V_{vdw}) of the bicalutamide and coformer molecules on the melting temperatures of the **Bic** cocrystals (Figure 7). It is evident that for the considered structures, the increase in T_{fus} of the cocrystals is accompanied by an increase in the van der Waals volume. The linear correlation coefficient for the data, however, is low (R = 0.912), which can be attributed to the following reasons: a) the van der Waals volume of **Bic** depends on a conformational state of the molecule in the crystal; b) thermal stability of the cocrystals is strongly affected by directional interactions such as hydrogen bonds, the strength of which is variable in the different structures. The general trend, however, remains clear: T_{fus} of the cocrystal increases as V_{vdw} of the molecules increases.

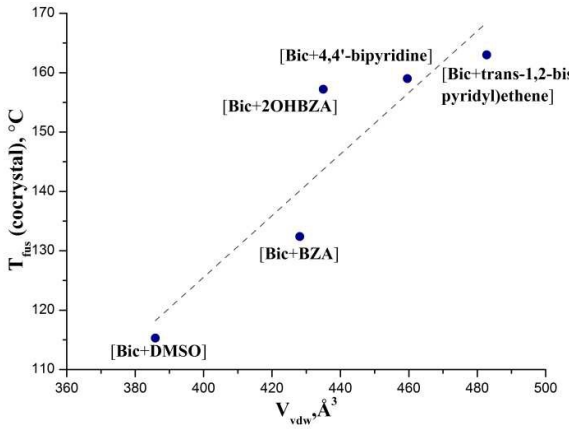

Figure 7 Dependence between melting points of the cocrystals and total van der Waals volume (V_{vdw}) of the molecules in the crystal asymmetric unit.

3.5 Solution stability and thermodynamics of the cocrystals formation

Formation of a cocrystal from the pure constituents is a thermodynamically favourable process, which is defined by a certain value of the Gibbs free energy change. The Gibbs energy, in turn, should be considered as a combination of enthalpy and entropy terms, and each provides important information concerning the relative strength of the intermolecular forces and order in a multicomponent system. It has been established that the Gibbs energy change at a given temperature can be evaluated from the solubility data of a cocrystal and its constituents in a particular solvent.[30,31] In order to obtain the enthalpy of formation, different experimental methods have been proposed. The first one is based on direct measurement of the heats of solution for a cocrystal and its pure components in a solvent by using solution calorimetry.[46-49] In the second method, the cocrystal's formation enthalpy is obtained as a difference of the melting enthalpies of a cocrystal and the physical mixture of its component crystals.[50-52] In our previous papers, an alternative approach towards the estimation of formation enthalpy has been applied.[53,54] In brief, this considered measuring the equilibrium constant for the formation reaction of a cocrystal using the procedure described in the *Material and Methods* section. The main advantage of this approach is that all of the thermodynamic parameters of the formation process (ΔG_f^0, ΔH_f^0, ΔS_f^0) can be obtained from the solubility data only using classical thermodynamic relationships.

Preliminary solubility experiments with 2 ml of a solvent showed that [**Bic**+**BZA**] and [**Bic**+**2OHBZA**] dissolve incongruently in methanol, acetonitrile, ethyl acetate and acetone to form pure bicalutamide in the bottom phase. The solubility values of **Bic**, **BZA** and **2OHBZA** in the latter solvents are shown in Table S1. The most significant difference in solubility of bicalutamide and coformers is observed in the polar protic solvent methanol: S^{2OHBZA}/S^{Bic} = 20.1, S^{BZA}/S^{Bic} = 39.5. In polar aprotic solvents (acetonitrile, ethyl acetate and acetone) the solubility ratio is considerably smaller, reaching the minimal value in acetone: S^{2OHBZA}/S^{Bic} = 4.8, S^{BZA}/S^{Bic} = 2.8. Thus, a ternary phase diagram in any of these solvents is expected to be asymmetric with narrow cocrystal stability regions. However, [**Bic**+**BZA**] and [**Bic**+**2OHBZA**] are found to dissolve congruently in less polar chloroform despite the significant difference in solubility of the components in the solvent: S^{2OHBZA}/S^{Bic} = 7.4, S^{BZA}/S^{Bic} = 31.1. The fact that cocrystals are stable in chloroform can be explained in terms of solute-solvent interaction energies (solvation energies), that should be much smaller in the solvent compared with more polar solvents. As a result, the cocrystal stability region in CHCl3 is wide enough to provide congruent dissolution, i.e. a cocrystal solubility curve in a ternary phase diagram crosses a cocrystal stoichiometric ratio line. The congruent solubility of the cocrystals was confirmed at each experimental temperature (18.0, 22.0, 25.0 and 30.0 ± 0.1 °C) by analyzing samples of the bottom phase using the DSC and PXRD methods. The experimental solubility values of the [**Bic**+**BZA**], [**Bic**+**2OHBZA**] cocrystals and their constituents in chloroform are shown in Table S2. The thermodynamic parameters of the cocrystals formation calculated according to equations (2), (4) and (5) are shown in Table 7.

Table 7. Standard thermodynamic functions of formation for [**Bic**+**BZA**] and [**Bic**+**2OHBZA**] cocrystals at 25.0 °C.

	ΔG_f^0, kJ·mol^{-1}	ΔH_f^0, kJ·mol^{-1}	ΔS_f^0, J·mol^{-1}·K^{-1}
[**Bic**+**BZA**]	–3.4 ± 0.3	–19.6 ± 0.8	–54 ± 4
[**Bic**+**2OHBZA**]	–2.2 ± 0.3	–11.4 ± 0.5	–31 ± 2

The negative values of the Gibbs energy suggest that formation of the cocrystals from individual components is a spontaneous process. It is shown that the ΔG_f^0 values for the [**Bic**+**BZA**] and [**Bic**+**2OHBZA**] cocrystals are comparable and relatively

small. However, the [**Bic**+**BZA**] formation enthalpy, ΔH_f^0, is found to be *ca* 8.2 kJ·mol^{-1} more exothermic than that of [**Bic**+**2OHBZA**], indicating that the crystal packing energy gain of a cocrystal relative to the individual components is greater for [**Bic**+**BZA**]. Since the thermodynamic parameters of formation of a multi-component compound are not a function of the solvent, it would be interesting to analyze the formation Gibbs energies available for different cocrystals and salts (Table 8).

Table 8. Thermodynamic parameters of formations for cocrystals and salts available in the literature

Multi-component compound	Type of system	T, °C[a]	ΔG_f^0, kJ·mol^{-1}	ΔH_f^0, kJ·mol^{-1}	$T\Delta S_f^0$, kJ·mol^{-1}	Solvent	Ref.
Carbamazepine–saccharin (1:1)	cocrystal	33	–4.6	–5.9	–1.5	Methanol	46
Carbamazepine–nicotinamide (1:1)	cocrystal	25	–4.8			Ethanol	30
Theophylline–oxalic acid (2:1)	cocrystal	30	–5.6			Chloroform/Methanol (4:1)	55
Theophylline−glutaric acid (1:1)	cocrystal	30	–0.4			Chloroform	56
Theophylline – salicylic acid (1:1)	cocrystal	30	–4.9			Chloroform	57
Benzoic acid – isonicotinamide (1:1)	cocrystal	20	–10.8			Ethanol	58
Adefovir dipivoxil – saccharin (1:1)	cocrystal	20	–12.1			Ethanol	59
Vanillin isoniazid – saccharin (1:1)	salt	25	–9.1	–13.5	–4.4	Water	53
Salinazid – saccharin (1:1)	salt	25	–7.3	–18.4	–11.0	Water	53

Table 8 indicates that most of the cocrystals have a relatively small driving force for formation, and the results for the bicalutamide cocrystals are in agreement with this trend. As mentioned above, complete information about thermodynamics of the formation process can be obtained by analyzing the enthalpy and entropy contributions to the Gibbs energy. The experimental results suggest that both bicalutamide cocrystals are enthalpy favored when compared with the parent components (Table 7). However, the relative contribution of the enthalpy term to the Gibbs energy comprises on average 55% (54.7% for [**Bic**+**BZA**] and 55.3% for [**Bic**+**2OHBZA**]). In the carbamazepine-saccharin (1:1) cocrystal, this value reaches ca 80%. In the salts of vanillin isoniazid and salinazid with saccharin, the enthalpy contribution equals ca 76% and 63%, respectively. Therefore, the relatively small value of ΔG_f^0 for the [**Bic**+**BZA**] and [**Bic**+**2OHBZA**] cocrystals should be attributed to a considerable decrease of the system entropy during the cocrystal formation. The negative ΔS_f^0 introduces a positive contribution to the Gibbs energy decreasing the driving force of the cocrystal formation process. As a result, the formation of the bicalutamide cocrystals is seen to be a consequence of the strong competition between ΔH_f^0 and ΔS_f^0 terms.

3.6 Aqueous dissolution of the bicalutamide cocrystals

The ultimate goal of cocrystallization for most APIs is to improve solubility, because it generally results in enhancement in bioavailability for a BCS class II API.[60] Dissolution experiments for the [**Bic**+**BZA**] and [**Bic**+**2OHBZA**] cocrystals were performed in pH 7.4 phosphate buffer, and the results are shown in Figure 8. The cocrystals are expected to dissolve incongruently in aqueous medium considering a significant difference in the solubilities of the pure components ($S^{2OHBZA}/S^{Bic} \approx 2000$, $S^{BZA}/S^{Bic} \approx 12000$).[61] As is seen, the dissolution profiles for both cocrystals demonstrate a classical so-called "spring and parachute" behavior.[23, 62-65] According to this concept, the "spring" effect is caused by fast dissociation of the cocrystal to form thermodynamically unstable, amorphous-like species of poorly soluble drug, whereas the longer-term "parachute" effect occurs because of slow crystallization of this amorphous material to stable crystalline phases in the presence of a well-soluble component. It has been reported that bicalutamide produces an amorphous state upon cooling of the melt, which is stable for a relatively long time even at room temperature.[20] This might be due to the conformational flexibility of the molecule and an associated energy barrier for crystallization. It can be assumed that rapid disruption of crystal lattices of the bicalutamide cocrystals during the dissolution process leads to formation of higher energy amorphous-like species of the drug, and an amount of time is required for these species to crystallize.

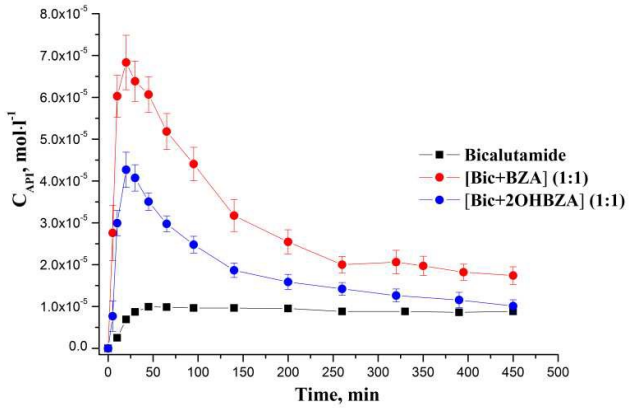

Figure 8 Dissolution profiles for the cocrystals and pure bicalutamide in the pH 7.4 phosphate buffer at 25°C. The error bar for pure Bic is within the size of square.

During the first ca. 20 min of the dissolution process of [**Bic**+**BZA**] and [**Bic**+**2OHBZA**] (the "spring" phase), the amount of Bic in the solution reaches its maximum value, which is approx. 7 and respectively 5 times higher compared to solubility of the parent form (Figure 8). This is followed by a longer-term "parachute" phase, when slow crystallization and precipitation of the unstable Bic species occur. The latter

process is accompanied by elevated concentration level and lasts for the following 7 hours. The XRPD analyses of the solid phases recovered after the dissolution experiments revealed transformation of the cocrystals to form pure bicalutamide form I. It has been reported that manipulation of the formulation by the addition of polymers or surfactants may inhibit the precipitation of the drug released from a cocrystal and thus sustain the state of drug supersaturation for a therapeutically relevant period of time in order for the drug to be absorbed.[66-72] We have recently found, however, that the extent of solubility enhancement achieved by some of these formulations may have the opposite effect on the permeability of an API.[73]

Conclusions

Cocrystal screening of the non-steroidal anti-androgen drug bicalutamide resulted in two new multicomponent solids with benzamide and salicylamide in a 1:1 molar ratio. Structural analyses revealed that both cocrystals contain similar molecular conformation of bicalutamide and show similar packing arrangements to form distinct layers consisting of hydrogen bonded tetrameric units. The results of *PIXEL* calculations indicated that total crystal lattice energies of the [**Bic**+**BZA**] and [**Bic**+**2OHBZA**] cocrystals are closely comparable. In both cocrystals, dispersion interactions dominate the crystal structures, while the Coulombic term also contributes significantly to the lattice energies, particularly in [**Bic**+**BZA**]. The main energy difference between the two cocrystals is observed for the bicalutamide–cocrystal former interaction energy, which is calculated to be slightly more stabilizing in [**Bic**+**BZA**]. According to the DSC results, the melting temperatures of the cocrystals are significantly lower than that of the pure API. It was found that the melting temperatures of all known bicalutamide cocrystals generally increase with an increase of the total van der Waals volume (V_{vdw}) of the molecules in the asymmetric unit of the crystal. With the solubility of the cocrystals and the corresponding solubility of the pure compounds in chloroform determined at different temperatures, the thermodynamic functions of the cocrystal formation were estimated. In both cases, the value of the Gibbs energy change of the process was found to be small: –3.4 $kJ \cdot mol^{-1}$ for [**Bic**+**BZA**] and –2.2 $kJ \cdot mol^{-1}$ for [**Bic**+**2OHBZA**]. The most significant contribution to the Gibbs energy is provided by the enthalpy of formation. However, the cocrystal formation is accompanied by a considerable decrease of the system entropy, which diminishes the driving force of the process. As a result, the formation of the bicalutamide cocrystals is seen to be a consequence of the strong competition between the enthalpy and entropy terms. Both cocrystals demonstrated a classical "spring and parachute" behavior during aqueous dissolution, providing an increased concentration level of **Bic** compared to that of the parent drug for several hours.

Acknowledgements

This work was supported by the Russian Scientific Foundation (№14-13-00640). We thank "the Upper Volga Region Centre of Physicochemical Research" for technical assistance with TG and XRPD experiments.

References

1 F. Ran, H. Xing, Y. Liu, D. Zhang, P. Li, and G. Zhao, *Arch. Pharm. (Weinheim).*, 2015, **348**, 757–775.
2 A. S. Waller, R. M. Sharrard, P. Berthon, and N. J. Maitland, *J. Mol. Endocrinol.*, 2000, **24**, 339–351.
3 F. Ren, Q. Jing, Y. Tang, Y. Shen, J. Chen, F. Gao, and J. Cui, *Drug Dev. Ind. Pharm.*, 2006, **32**, 967–972.
4 I. D. Cockshott, *Clin. Pharmacokinet.,* 2004, **43**, 855–878.
5 G. P. Andrews, A. A. Osama, D. S. Jones, *J. Pharm. Sci.* 2010, **99**, 1322–1335.
6 O. A. Abu-Diak, D. S. Jones, and G. P. Andrews, *J. Pharm. Sci.*, 2012, **101**, 200–213.
7 K. B. Narkhede, R. B. Laware, Y. P. Sharma, S. S. Rawat, *Pharma Science Monitor - An International Journal of Pharmaceutical Sciences,* 2012, **3**, 2739–2748.
8 F. Tres, S. R. Coombes, A. R. Phillips, L. P. Hughes, S. A. C. Wren, J. W. Aylott, and J. C. Burley, *Molecules*, 2015, **20**, 16404–16418.
9 F. Tres, J. D. Patient, P. M. Williams, K. Treacher, J. Booth, L. P. Hughes, S. A. C. Wren, J. W. Aylott, and J. C. Burley, *Mol. Pharm.*, 2015, **12**, 1512–1522.
10 Y. Le, H. Ji, J. F. Chen, Z. Shen, J. Yun, and M. Pu, *Int. J. Pharm.*, 2009, **370**, 175–180.
11 T. A. Meer, K. P. Sawant, and P. D. Amin, *Acta Pharm.*, 2011, **61**, 435–445.
12 C. Li, C. Li, Y. Le, and J. F. Chen, *Int. J. Pharm.*, 2011, **404**, 257–263.
13 D. D. Kumbhar and V. B. Pokharkar, *Colloids and Surfaces A: Physicochem. Eng. Aspects,* 2013, **416**, 32–42.
14 R. Kudarha, N. L. Dhas, A. Pandey, V. S. Belgamwar, and P. P. Ige, *Pharm. Dev. Technol.*, 2015, **20**, 608–618.
15 J. Guo, S. Wu, W. Ren, X. Wang, and A. Yang, *Exp. Ther. Med.*, 2015, 2305–2310.
16 N. L. Dhas, P. P. Ige, and R. R. Kudarha, *Powder Technol.*, 2015, **283**, 234–245.
17 A. A. Smith, K. Kannan, R. Manavalan, and N. Rajendiran, *J. Incl. Phenom. Macrocycl. Chem.*, 2007, **58**, 161–167.
18 M. V. Srikanth, G. V. Murali Mohan Babu, N. S. Sreenivasa Rao, S. A.Sunil, K. V. Ramanamurthy, *Int. J. Pharm. Pharm. Sci.*, 2010, **2**, 191–198.
19 D. R. Vega, G. Polla, A. Martinez, and E. Mendioroz, *Int. J. Pharm.*, 2007, **328**, 112–118.
20 Z. Német, J. Sztatisz, A. Demeter, *J. Pharm. Sci.*, 2008, **97**, 3222–3232.
21 G. L. Perlovich, S. V. Blokhina, N. G. Manin, T. V. Volkova, and V. V. Tkachev, *J. Therm. Anal. Calorim.*, 2013, **111**, 655–662.
22 N. Schultheiss and A. Newman, *Cryst. Growth Des.*, 2009, **9**, 2950–2967.
23 N. J. Babu and A. Nangia, *Cryst. Growth Des.*, 2011, **11**, 2662–2679.
24 J. Bis, P. Vishweshwar, D. Weyna, and M. J. Zaworotko, *Mol. Pharm.*, 2007, **4**, 401–416.
25 T. Friščić, S. L. Childs, S. A. A. Rizvic, W. Jones, *CrystEngComm*, 2009, **11**, 418–426.

26 S. Aher, R. Dhumal, K. Mahadik, A. Paradkar, and P. York, *Eur. J. Pharm. Sci.*, 2010, **41**, 597–602.
27 A. Newman, *Org. Process Res. Dev.*, 2013, **17**, 457–471.
28 G. M. Sheldrick, *Acta Crystallogr., Sect. A: Found. Crystallogr.*, 2008, **64**, 112-122.
29 A. L. Spek, *Acta Crystallogr., Sect. D Biol. Crystallogr.* 2009, **65**, 148–155.
30 R. R. Schartman, *Int. J. Pharm.,* 2009, **365**, 77-80.
31 T. Rager and R. Hilfiker, *Z. Phys. Chem.*, 2009, **223**, 793-813.
32 A. Gavezzotti, *Mol. Phys.*, 2008, **106**, 1473–1485.
33 L. Maschio, B. Civalleri, P. Ugliengo, and A. Gavezzotti, *J. Phys. Chem. A*, 2011, **115**, 11179–11186.
34 E. Lu, N. Rodríguez-Hornedo, and R. Suryanarayanan, *CrystEngComm*, 2008, **10**, 665-668.
35 H. Yamashita, Y. Hirakura, M. Yuda, and K. Terada, *Pharm. Res.*, 2014, **1**, 1–12.
36 A. N. Manin, A. P. Voronin, K. V. Drozd, N. G. Manin, A. Bauer-Brandl, and G. L. Perlovich, *Eur. J. Pharm. Sci.*, 2014, **65**, 56–64.
37 M. C. Etter, *Acc. Chem. Res.* 1990, **23**, 120 – 126
38 J. Bernstein, R. E. Davis, L. Shimoni, N-L. Chang, *Angew. Chem. Int. Ed. Engl.* 1995, **34**, 1555 – 1573.
39 D. K. Dhaked, V. Jain, Y. Kasetti, and P. V. Bharatam, *Struct. Chem.*, 2012, **23**, 1857–1866.
40 M. K. Stanton, S. Tufekcic, C. Morgan, and A. Bak, *Cryst. Growth Des.,* 2009, **9**, 1344–1352.
41 L. Orola, M. V. Veidis, I. Mutikainen, and I. Sarcevica, *Cryst. Growth Des.*, 2011, **11**, 4009–4016.
42 C. B. Aakeröy, S. Forbes, and J. Desper, *CrystEngComm*, 2012, **14**, 2435- 2443.
43 I. Sarcevica, L. Orola, M. V. Veidis, A. Podjava, and S. Belyakov, *Cryst. Growth Des.*, 2013, **13**, 1082–1090.
44 C. B. Aakeröy, S. Forbes, and J. Desper, *CrystEngComm*, 2014, **16**, 5870–5877.
45 G. L. Perlovich, *CrystEngComm*, 2015, **17**, 7019-7028.
46 M. A. Oliveira, M. L. Peterson, and R. J. Davey, *Cryst. Growth Des.*, 2011, **11**, 449–457.
47 R. Chadha, A. Saini, P. Arora, D. S. Jain, A. Dasgupta, and T. N. G. Row, *CrystEngComm*, 2011, **13**, 6271–6284.
48 A. O. L. Évora, R. A. E. Castro, T. M. R. Maria, M. R. Silva, J. H. Ter Horst, J. Canotilho, and M. E. S. Eusébio, *Int. J. Pharm.*, 2014, **466**, 68–75.
49 A. O. Surov, A. P. Voronin, A. N. Manin, N. G. Manin, L. G. Kuzmina, A. V. Churakov, and G. L. Perlovich, *Mol. Pharm.*, 2014, **11**, 3707–3715.
50 S. W. Zhang, I. A. Guzei, M. M. De Villiers, L. Yu, and J. F. Krzyzaniak, *Cryst. Growth Des.*, 2012, **12**, 4090–4097.
51 S. W. Zhang, J. Kendrick, F. J. J. Leusen, and L. Yu, *J. Pharm. Sci.*, 2014, **103**, 2896–2903.
52 Y. Yan, J.-M. Chen, and T.-B. Lu, *CrystEngComm*, 2015, **17**, 612–620.
53 A. O. Surov, A. P. Voronin, A. A. Simagina, A. V. Churakov, S. Y. Skachilova, and G. L. Perlovich, *New J. Chem.*, 2015, **39**, 8614–8622.
54 A. O. Surov, A. N. Manin, A. V. Churakov, and G. L. Perlovich, *Mol. Pharm.*, 2015, **12**, 4154–4165.
55 S. Zhang and A. C. Rasmuson, *CrystEngComm*, 2012, **14**, 4644–4655.
56 S. Zhang and Å. C. Rasmuson, *Cryst. Growth Des.*, 2013, **13**, 1153–1161.
57 S. Zhang, H. Chen, Å. C. Rasmuson. *CrystEngComm* **2015**, **17**, 4125-4135
58 S. Boyd, K. Back, K. Chadwick, R. J. Davey, and C. C. Seaton, *J. Pharm. Sci.*, 2010, **99**, 3779–3786.
59 K. Ma, Y. Zhang, H. Kan, L. Cheng, L. Luo, Q. Su, J. Gao, Y. Gao, and J. Zhang, *Pharm. Res.*, 2014, **31**, 1766–1778.
60 N. Shan, M. L. Perry, D. R. Weyna, and M. J. Zaworotko, *Expert Opin. Drug Metab. Toxicol.*, 2014, **10**, 1–17.
61 S. H. Yalkowsky, Y. He, P. Jain, Handbook of Aqueous Solubility Data, Second Edition. CRC Press: Boca Raton, 2010.
62 R. Thakuria, A. Delori, W. Jones, M. P.Lipert, L. Roy, N. Rodriguez-Hornedo, *Int. J. Pharm.,* 2013, **453**, 101–125
63 A. J. Smith, P. Kavuru, L. Wojtas, M. J. Zaworotko, and R. D. Shytle, *Mol. Pharm.*, 2011, **8**, 1867–1876.
64 L. L. Xu, J. M. Chen, Y. Yan, and T. B. Lu, *Cryst. Growth Des.*, 2012, **12**, 6004–6011.
65 J. X. Song, J. M. Chen, and T. B. Lu, *Cryst. Growth Des.*, 2015, **15**, 4869–4875.
66 J. F. Remenar, M. L. Peterson, P. W. Stephens, Z. Zhang, Y. Zimenkov, and M. B. Hickey, *Mol. Pharm.*, 2007, **4**, 386–400.
67 S. L. Childs, P. Kandi, and S. R. Lingireddy, *Mol. Pharm.*, 2013, **10**, 3112–3127.
68 A. Alhalaweh, H. R. H. Ali, and S. P. Velaga, *Cryst. Growth Des.*, 2014, **14**, DOI: 10.1155/2015/870656.
69 M. Ullah, H. Ullah, G. Murtaza, Q. Mahmood, and I. Hussain, *Biomed Res. Int.*, 2015, **2015**.
70 S. Baghel, H. Cathcart, and N. J. O'Reilly, *J. Pharm. Sci.*, 2016. DOI: 10.1016/j.xphs.2015.10.008
71 L. Sousa, S. M. Reutzel-Edens, G. A. Stephenson, and L. S. Taylor, *Cryst. Growth Des.*, 2016, **16**, 737–748.
72 C. Liu, Z. Chen, Y. Chen, J. Lu, Y. Li, S. Wang, G. Wu, and F. Qian, *Mol. Pharm.*, 2016, **13**, 599–608.
73 S. Yui, K. Fong, S. M. Martins, M. Brandl, and A. Bauer-brandl, *J. Pharm. Sci.*, 2016, **3549**, 1–11.